FULL PAPER

ADVANCED FUNCTIONAL MATERIALS

Hierarchical Pattern Formation in Thin Polymer Films Using an Electric Field and Vapor Sorption**

By *Stephan Harkema* and *Ullrich Steiner**

The experimental observation of electric-field-induced instabilities of polymer films exposed to toluene vapors is reported. When using a laterally structured electrode, the pattern that forms in the polymer film is governed by the interplay of the intrinsic film instability and the periodicity of the electrode structure. By adjusting the applied voltage, it is possible to switch between two different pattern-replication modes. A further important parameter is the aspect ratio of the structured electrode. For high ratios of polymer film thickness to capacitor-plate spacing, structures with hierarchical length scales have been observed.

1. Introduction

The control of pattern-formation processes on surfaces and in thin films is of increasing importance for technological applications ranging from semiconductor lithography to the controlled modification of mechanical and optical aspects of surfaces. In addition to the traditional lithographic approaches of photolithography and electron-beam lithography, a number of soft-lithographic techniques enjoy an increasing popularity.[1] Very recently, capillary instabilities of liquid surfaces have been employed.[2–5] By applying a laterally inhomogeneous pressure to a liquid film, surface instabilities can be guided to replicate a master structure.

Soft-lithographic techniques require the initial liquifaction and subsequent solidification of a resist material. This is typically achieved by using polymer solutions, from which the solvent is evaporated during a molding process or by heating and subsequently cooling of the sample. A less commonly used strategy is the liquefaction of a glassy polymeric material by the absorption of vapor from a solvent atmosphere.[6] Vapor-absorption experiments have a number of advantages. As opposed to evaporating solutions, the amount of solvent in the material can be controlled by adjusting the surrounding solvent vapor pressure and, thereby, the viscosity of the liquefied polymer. Heating a polymer film above the glass-transition temperature, on the other hand, results in a highly viscous melt (and therefore in slow pattern-formation kinetics) and an increased degradation of the polymer by thermal oxidation.

The liquefaction of polymers by the absorption of solvent vapor is well understood.[6] Similar to an increase in temperature, the diffusion of a low-molecular-weight solvent into a polymer matrix results in an increase in free volume, thereby lowering the glass-transition temperature.[7] Chow derived an expression for the depression of the glass-transition temperature with increasing diluent concentration in the polymer.[7] For polystyrene (PS), a toluene uptake of 14 % (by weight) is sufficient to lower the glass-transition temperature to room temperature,[8] making vapor sorption an interesting alternative to thermal annealing.

While the modification of polymer properties by solvents is known from a number of engineering applications,[9–13] solvent annealing is an increasingly popular strategy to study relaxation phenomena in thin polymer films. It is mainly used to examine the ordering of copolymer morphologies in thin films.[14–18]

Here, this strategy is applied to the structure formation of homopolymer films exposed to electric fields. The application of an electric field normal to a liquid surface causes a rippling of the initially flat surface.[19] Capillary waves of a well-defined wavelength grow with time. In the confinement of a plate capacitor, this leads to liquid cylindrical bridges spanning the two capacitor plates with a lateral periodicity that is given by the wavelength λ_i of the initially amplified wave spectrum.[20] Since the pattern selection is dominated by the initial phase of the instability, λ_i is quantitatively described by a linear stability analysis.[21,22]

This electrohydrodynamic (EHD) pattern-formation process can be employed to lithographically replicate submicrometer-sized structures.[2] This is achieved by a lateral variation of the applied electric field. The film wave maxima are drawn towards locations of highest electric-field strength, and thus the film replicates the field-density profile. The lateral field-density variation is typically achieved by using a patterned conducting surface as master template. In this work, this approach was modified, using a patterned dielectric layer (made from a cross-linked epoxy resin) on top of a planar electrode as master template (Fig. 1).

[*] Prof. U. Steiner
Department of Physics, Cavendish Laboratory, University of Cambridge
Madingley Road, Cambridge CB3 0HE (UK)
E-mail: u.steiner@phy.cam.ac.uk
S. Harkema
Department of Polymer Chemistry and Materials Science Center
University of Groningen
Nijenborgh 4, NL-9747 AG Groningen (The Netherlands)

[**] We thank J. Heier for the manufacture of the patterned epoxy plates. This work was partially funded by the Dutch Stichting voor Fundamenteel Onderzoek der Materie (FOM) and by BioMaDe. Supporting Information is available online from Wiley InterScience or from the author.

  DOI: 10.1002/adfm.200500388

ADVANCED FUNCTIONAL MATERIALS

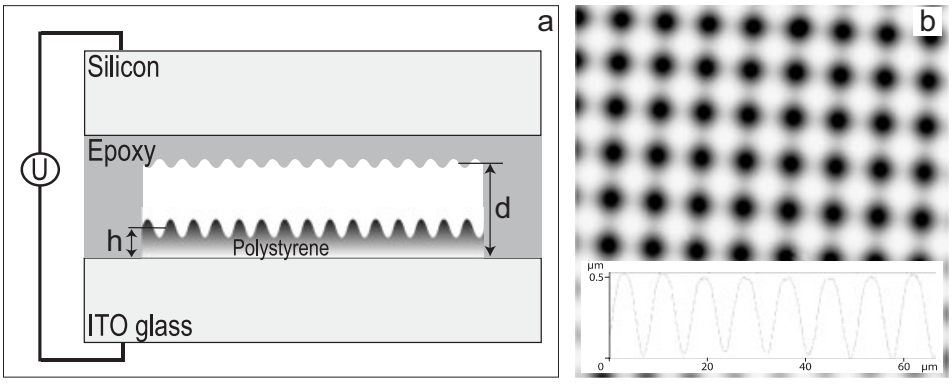

Figure 1. a) Schematic representation of the experimental setup. A liquid polymer film is destabilized by an electric field generated by an applied voltage, *U*. The top plate has a dielectric sinusoidal pattern with a wavelength of 6 µm. To adjust the distance between the electrodes, spacers are added with a lateral spacing of 500 µm; ITO: indium tin oxide. b) Atomic force microscopy (AFM) image of the epoxy pattern of the top plate. The bottom image is a cross-section profile along a diagonal of the square lattice.

The patterns that form in such a structured electric field are determined by the interplay of the two lateral length scales that are intrinsic to this experiment: 1) the destabilization wavelength, λ_i, which is determined by the balance of the destabilizing electrostatic pressure gradient and the restoring interfacial tension; and 2) the periodicity of the epoxy master template, λ_m. In particular, we show that the replicated pattern size can be switched discretely by adjusting the applied voltage. A second aspect that leads to a hierarchical pattern-formation process arises from the annealing of the film in a solvent-vapor atmosphere. As opposed to thermal annealing (where the volume of the resist changes only very little during the quench below the glass-transition temperature), the solidification of the film by drying in solvent-free air leads to a volume contraction by approximately 40 %. This leads to the lateral contraction of the replicated pattern, often giving rise to a secondary pattern-formation process.

2. Results and Discussion

EHD film destabilization is determined by a force balance at the liquid surface between the destabilizing electrostatic pressure (p_{es}) gradient and the restoring surface tension γ.[20] In the long-wavelength limit (film undulation amplitude $\ll \lambda_i$), the pattern selection is given by

$$\lambda_i = 2\pi\sqrt{\frac{\gamma}{-\partial p_{es}/\partial h}} \quad (1)$$

where h is the film thickness. The magnitude of the variation of p_{es} with h depends on U and the capacitance per unit area, C; Equation 1 can then be written as:

$$\lambda_i = 2\pi c_{\varepsilon_p}\sqrt{\gamma\frac{\varepsilon_0^2}{U^2C^3}} \quad (2)$$

where ε_0 is the dielectric vacuum permittivity. For plane-parallel capacitor plates, the constant $c_{\varepsilon_p} = \varepsilon_p/(\varepsilon_p - 1)$ is weakly dependent on the dielectric constant of the polymer ε_p. C is given by the inverse summation rule for three capacitors connected in series (polymer–air–epoxy, see Fig. 1a).

For the setup shown in Figure 1a, λ_i is determined by the applied voltage, the capacitor-plate spacing, and the film thickness. Since γ and ε_p of PS change only very little upon swelling (< 3 %), the value of λ_i is comparable to that obtained from similar experiments in which the PS film was liquefied by heating. The advantage of the swelling experiment lies in the dynamics of film destabilization. The characteristic time for film destabilization, τ_i, scales linearly with the film viscosity, which is greatly reduced in the swollen film.

Figure 2 shows optical and atomic force microscopy (AFM) images of a PS film at various stages of EHD destabilization. Despite the use of spacers to maintain a constant plate spacing, a small variation of the interplate spacing (on the order of 2 µm cm^{-1}) was typically observed. This led to a lateral variation of the capacitance. Both λ_i and τ_i are functions of the lateral sample position. It is therefore possible to observe various stages of the EHD instability on the same sample.

Figure 2a shows the early stage of film instability. The sinusoidal undulations of the PS film faithfully mirror the pattern of the epoxy master. With time, the undulations grew and made contact with the epoxy protrusions (Fig. 2b). In addition to these polymer columns, small amounts of PS are discernible on the interstitial sites. Apart from the replication of the master pattern, replication defects are clearly visible in Figure 2a.

While some of these defects may arise from impurities in the polymer film leading to defect nucleation, most of these irregularities are intrinsic to the pattern-replication process. The field in the capacitor can be described as a homogeneous mean field with a superposed square-lattice lateral structure. The homogeneous mean component of the field gives rise to an EHD instability with an intrinsic wavelength λ_i given by Equation 2, while the lateral electric-field variation leads to the surface pattern with λ_m shown in Figure 2a. The pattern that forms in the polymer film is determined by the interplay of these two destabilizing effects.

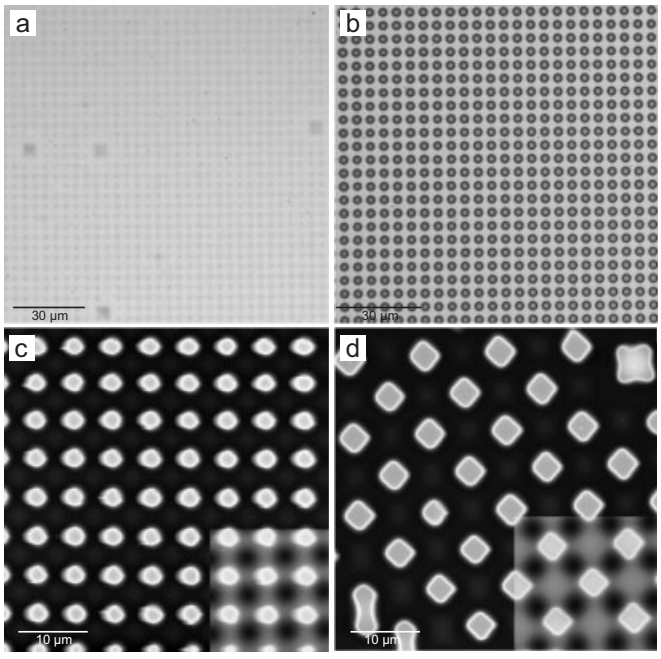

Figure 2. EHD replication of the electrode pattern in Figure 1 into a PS film. The optical micrographs in (a,b) show the early and late stages of the replication process, respectively. The replication defects arise from a mismatch of the intrinsic destabilization wavelength and the pattern periodicity. The AFM images in (c,d) correspond to the cases $\lambda_i \approx \lambda_m$ and $\lambda_i > \lambda_m$, respectively. For the large mismatch of the two length scales in (d) only every second lattice point is replicated. The insets show overlays of the master pattern of Figure 1b.

The patterns resulting from this interplay are shown in the AFM images in Figures 2c,d. The parameters that led to the PS patterns in both images were similar, but the applied voltage differed by a factor of two. This led to a change in the destabilizing pressure gradient by a factor of four and a change in λ_i by a factor of two (Eq. 2). For an applied voltage of 80 V, the results of which are shown in Figure 2c, the replicated PS columns coincide with each of the points of the square lattice. In this experiment, the intrinsic instability wavelength $\lambda_i \approx 8.1$ μm was comparable to the lattice spacing of $\lambda_m = 6$ μm. Lowering the voltage to 40 V, the results of which are shown in Figure 2d, caused an increase in the EHD wavelength to $\lambda_i \approx 20.2$ μm. The large mismatch between λ_i and λ_m resulted in a different pattern selection. Instead of completely replicating the master electrode, the PS columns occupied alternating lattice positions with unoccupied interstitial lattice points. This led to a replicated symmetry, which was rotated by 45° with respect to the epoxy master, and a lattice spacing of $\lambda_d = \sqrt{2\lambda_m^2} \approx 8.5$ μm, corresponding to the diagonal of the master pattern.

Figures 2c,d show that different replication patterns can be selected by adjusting the mismatch of λ_i and λ_m This is shown for a larger data set in Figure 3a. For $\lambda_i < 2\lambda_m$ the complete replication mode of Figure 2c is selected, while for $\lambda_i > 2\lambda_d$, the pattern found in Figure 2d is reproduced. For $2\lambda_m < \lambda_i < 2\lambda_d$ patterns similar to Figure 4b are observed, i.e., incomplete replication of the square lattice, which can be interpreted in terms of a coexistence of the patterns from Figures 2c,d.

Since the transition in pattern selection can be triggered by the applied voltage, it is possible to switch between these two pattern-replication modes during a single experimental run. The results of this are shown in Figure 4a. There was a small increase in capacitor-plate spacing (by ≈ 18 nm) from the bottom-left to the top-right of Figure 4a. This caused a pattern-replication process that propagated with time along this gradient. For an applied voltage of 40 V, a pattern with $\lambda_m = 8.5$ μm in the lower-left part of Figure 4a was formed, while the PS film in the upper half of the sample remained stable. Once the pattern-replication front had reached the shaded part of Figure 4a, the voltage was increased to 80 V. This caused the transition in pattern selection to $\lambda_m = 6$ μm, as the replication proceeded in the upper part of the sample.

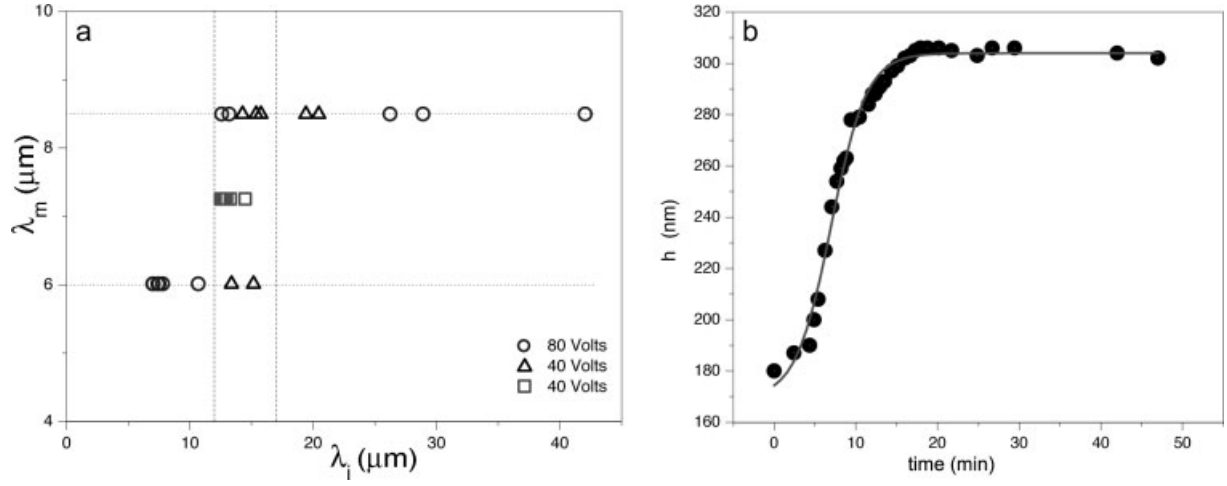

Figure 3. a) Replication of a square lattice as a function of the wavelength of the intrinsic (laterally averaged) instability wavelength λ_i. The two plateau values of λ_m correspond to lattice constants of 6 and 8.5 μm (diagonal). The squares stem from patterns similar to Figure 4b, which span several lattice points. b) Optical thickness on swelling of a 180 nm thick PS film in a saturated toluene atmosphere, as determined by ellipsometry.

ADVANCED FUNCTIONAL MATERIALS

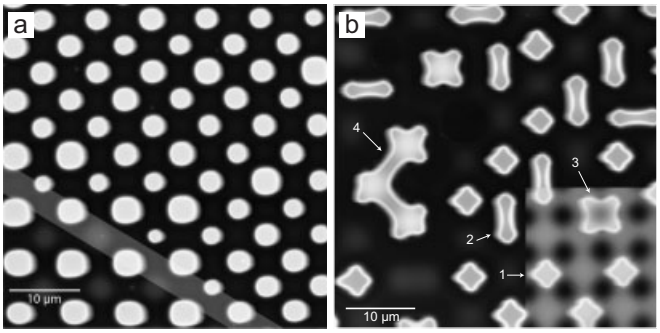

Figure 4. AFM images showing hierarchal EHD pattern replication. a) By doubling the applied voltage during pattern replication (shaded stripe), it is possible to switch from the morphology of Figure 2d to the fully replicated pattern of Figure 2c. b) When using an epoxy master with a smaller grid amplitude, columns that span more than one lattice point were observed (1); cross-shaped columns arise from the pinning of the deswelling columns on the ridges connecting the master protrusions. Elongated (2) and x-shaped (3) columns stem from PS plugs spanning two and four columns, respectively, with larger coalesced structures (4). The inset shows an overlay of the master pattern of Figure 1b.

A further mode in pattern replication is shown in Figure 4b. A small plate spacing (d =620 nm) combined with a low applied voltage (40 V) led to PS plugs that spanned more than one electrode protrusion. The branched patterns in Figure 4b are a consequence of large PS plugs in the swollen state and their shrinkage upon drying the sample. In all experiments, after the solvent atmosphere was replaced with air, evaporation of the toluene from the columns led to lateral shrinkage of the columns, since vertical shrinkage is suppressed because of the pinning of the plugs to the electrode surfaces. Columns that were pinned to a single epoxy protrusion of the master electrode contracted isotropically. This led to the nearly circular cross-sections of the columns shown in Figure 2c. Plugs that span more than one epoxy protrusion have non-circular cross-sections even in the swollen state. Upon drying, the lateral contraction led to the patterns with partially concave cross-sections in Figure 4b. Four different morphologies were observed. The cross-shaped morphology (1) arose from a (in the swollen state) large diameter column that made contact to the epoxy ridges connecting the protrusions of the top plate in a square lattice. Upon deswelling, the contact line was pinned at these ridges, giving rise to the cross-shaped cross-section. In (2), a swollen column has made contact with two epoxy protrusions, leading to the elongated concave structures upon deswelling. Swollen columns that share four epoxy protrusions give rise to star-shaped structures (3). Combinations of these three structural elements cause larger plug-shaped PS regions, such as (4), with larger and more complex patterns on other parts of the sample.

The main difference between Figure 4b and the more direct replication of Figure 2 is the filling ratio of the capacitor gap. For a high filling ratio, h/d, the PS columns remain interconnected by a polymer film on the substrate for a considerable time after their initial formation. This allows the lateral redistribution of material (e.g., lateral Ostwald ripening). As opposed to lower h/d ratios, where the columns become isolated early on, this gives rise to large plug-shaped structures. After deswelling, this causes the morphologies with partially concave cross-sections shown in Figure 4b.

3. Conclusions

Based on earlier work on EHD pattern replication, several new concepts are introduced in the present article. 1) We have shown that annealing of polymer films in a solvent vapor during EHD pattern formation is a versatile and robust alternative to the more commonly used temperature-annealing approach. Beneficial is, in particular, the low viscosity of the swollen polymer, which significantly reduces the time required for pattern replication. 2) By carefully tuning the interplay of the intrinsic wavelength λ_i and the periodicity of the template patterns, two different replication modes can be selected. Depending on the pattern symmetry, it is likely that this pattern-selection mechanism can be further extended. 3) By superposing a lateral variation of the electrode spacing with the pattern-selection process, it is possible to switch between the two pattern-replication modes in a single experimental run. This is an interesting strategy for the manufacture of patterns with hierarchical lateral length scales. 4) A further important parameter in pattern selection is the filling ratio of the capacitor gap. Small filling ratios lead to the faithful replication of the master electrode and high filling ratios give rise to laterally coalesced structures. While the patterns in Figure 4b may be detrimental when the faithful replication of patterns is required, they could possibly be of use in a hierarchical approach, when widely varying lateral length scales have to be replicated.

4. Experimental

The polymer used was PS with a weight-average molecular weight of $M_w = 515\ \mathrm{kg\,mol^{-1}}$ ($M_w/M_n < 1.06$; M_n = number-average molecular weight) (Polymer Standards Service, Mainz, Germany). Indium tin oxide (ITO)-covered glass slides with a resistivity of $\approx 112\ \Omega\,\mathrm{cm^{-1}}$ were used as substrates. The glass slides were cleaned in a jet of CO_2 ice crystals (snow-jet) prior to film deposition. 180 nm thick PS films were deposited by spin-casting from a toluene solution.

A schematic representation of the experimental setup is shown in Figure 1a. The top plate consisted of a silicon wafer covered with a patterned epoxy layer. Also included on the top plate were spacer structures to control the sample–top plate distance. The details of the top-plate manufacture will be described elsewhere [23]. Figure 1b shows an AFM image of the epoxy structure. It consists of a square-lattice sinusoidal pattern with a periodicity $\lambda_m = 6$ µm. The structured silicon wafer was mounted facing the polymer film. Spacers at lateral distances of 500 µm assured a separation of ≈ 600 µm between the film and the epoxy pattern. Both capacitor plates were electrically contacted using silver paint (Electrodag 1415M) and the assembly was placed into a sealed chamber on top of an inverted optical microscope (Olympus GX 61).

The experiment was started by introducing a saturated toluene atmosphere into the chamber, inducing swelling of the polymer film, while the capacitor plates were electrically grounded. After 15 min, a voltage of 40 V was applied to the electrodes for 15 min and was then increased to 80 V for another 15 min. The polymer structure was then

solidified by exchanging the toluene-saturated atmosphere for air and the sample was dried for 30 min. The EHD structure formation of the polymer film was monitored and recorded by the microscope and a connected computer throughout the experiment. After removal of the top plate, the quenched polymer film was further characterized by optical microscopy (Olympus BX60) and by AFM (Veeco Dimension 3100).

In a separate experiment, the swelling of a PS film in a saturated toluene atmosphere was characterized using a single-wavelength imaging ellipsometer (Nanofilm EP3). The thickness change of the film as a function of time, calculated from the ellipsometric angles, is shown in Figure 3b. In a saturated toluene atmosphere, the initially 180 nm thick film swelled to 305 ±2 nm within ≈ 15 min. The refractive index is estimated to change from 1.59 to 1.55 during the swelling of the film, corresponding to a refractive index change of ≈ 3 %. The swelling experiment is of importance, since the interpretation of the EHD instability depends on the parameters (film thickness, dielectric constant) of the swollen film.

Received: June 23, 2005
Final version: July 21, 2005
Published online: October 19, 2005

[1] Y. Xia, J. A. Rogers, K. E. Paul, G. M. Whitesides, *Chem. Rev.* **1999**, *99*, 1823.
[2] E. Schäffer, T. Thurn-Albrecht, T. P. Russell, U. Steiner, *Nature* **2000**, *403*, 874.
[3] E. Schäffer, S. Harkema, M. Roerdink, R. Blossey, U. Steiner, *Adv. Mater.* **2003**, *15*, 514.
[4] S. Harkema, E. Schäffer, M. D. Morariu, U. Steiner, *Langmuir* **2003**, *19*, 9714.
[5] S. Y. Chou, L. Zhuang, L. Guo, *Appl. Phys. Lett.* **1999**, *75*, 1004.
[6] J. D. Ferry, *Viscoelastic Properties of Polymers*, John Wiley and Sons, New York **1980**.
[7] T. S. Chow, *Macromolecules* **1980**, *13*, 362.
[8] A. Laschitsch, C. Bouchard, J. Habicht, M. Schimmel, J. Rühe, D. Johannsmann, *Macromolecules* **1999**, *32*, 1244.
[9] P. P. Singh, D. E. Maier, J. H. Cushman, K. Haghighi, C. Corvalan, *J. Math. Biol.* **2004**, *49*, 1.
[10] E. N. Hoggan, K. Wang, D. Flowers, J. M. DeSimone, R. G. Carbonell, *IEEE Trans. Semicond. Manufact.* **2004**, *17*, 510.
[11] N. H. Jalani, P. Choi, R. Datta, *Solid State Ionics* **2004**, *175*, 815.
[12] B. Narasimhan, *Adv. Drug Delivery Rev.* **2001**, *48*, 195.
[13] J. R. Royer, Y. J. Gay, J. M. DeSimone, S. A. Khan, *J. Polym. Sci., Part B: Poly. Phys.* **2000**, *38*, 3168.
[14] H. Elbs, C. Drummer, V. Abetz, G. Krausch, *Macromolecules* **2002**, *35*, 5570.
[15] A. Knoll, A. Horvat, K. S. Lyakhova, G. Krausch, G. J. A. Sevink, A. V. Zvelindovsky, R. Margerle, *Phys. Rev. Lett.* **2002**, *89*, 035 501.
[16] N. Rehse, A. Knoll, R. Magerle, G. Krausch, *Macromolecules* **2003**, *36*, 3261.
[17] A. Knoll, R. Magerle, G. Krausch, *J. Chem. Phys.* **2004**, *120*, 1005.
[18] H. Elbs, G. Krausch, *Polymer* **2004**, *45*, 7935.
[19] J. R. Melcher, *Field-Coupled Surface Waves*, MIT Press, Cambridge, MA **1963**.
[20] E. Schäffer, T. Thurn-Albrecht, T. P. Russell, U. Steiner, *Europhys. Lett.* **2001**, *53*, 518.
[21] A. Vrij, *Discuss. Faraday Soc.* **1966**, *42*, 23.
[22] F. Brochard-Wyart, F. J. Daillant, *Can. J. Phys.* **1990**, *68*, 1084.
[23] J. Heier, S. Harkema, N. E. Voicu, U. Steiner, unpublished.

